ACS APPLIED MATERIALS & INTERFACES

Research Article

www.acsami.org

Highly Efficient Organic Photovoltaics via Incorporation of Solution-Processed Cesium Stearate as the Cathode Interfacial Layer

Guojie Wang,[†,‡] Tonggang Jiu,*[,†] Chunming Sun,[†] Jun Li,[†] Pandeng Li,[†] Fushen Lu,*[,‡] and Junfeng Fang*[,†]

[†]Institute of New Energy Technology, Ningbo Institute of Material Technology and Engineering (NIMTE), Chinese Academy of Science (CAS), Ningbo, Zhejiang 315201, P. R. China

[‡]Department of Chemistry, College of Science, Shantou University, Shantou, Guangdong 515063, P. R. China

Supporting Information

ABSTRACT: Highly efficient organic solar cells were successfully demonstrated by incorporating a solution-processed cesium stearate between the photoactive layer and metal cathode as a novel cathode interfacial layer. The analysis of surface potential change indicated the existence of an interfacial dipole between the photoactive layer and metal electrode, which was responsible for the power conversion efficiency (PCE) enhancement of devices. The significant improvement in the device performance and the simple preparation method by solution processing suggested a promising and practical pathway to improve the efficiency of the organic solar cells.

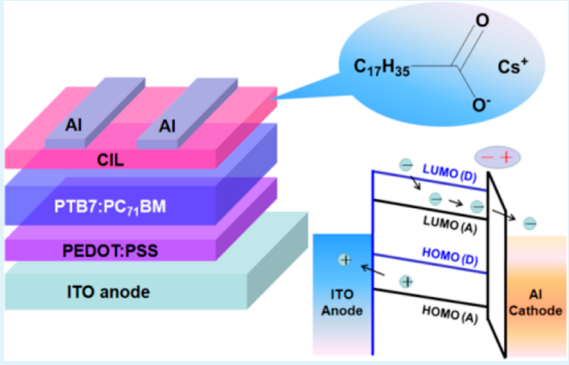

KEYWORDS: *organic solar cells, cesium stearate, interfacial layer, efficiency, solution-processed*

INTRODUCTION

Solution-processed bulk heterojunction (BHJ) organic photovoltaics (OPVs) have attracted considerable interest during the past few years as a promising source of renewable energy because of their unique advantages such as low cost and being lightweight, flexible, and compatible with large-area manufacturing technology.[1−6] A typical BHJ device, consisting of a phase separated blend of electron donor and acceptor materials as the photoactive layer, has a significant advantage in that a great proportion of the excitons are within the diffusion length of the donor−accept interface. With the development of materials design and interface control, as well as the optimization of device structure and fabrication process, the power conversion efficiencies (PCEs) of BHJ devices have been remarkably improved.[7−14] For example, PCEs of 9.2% and 8.2% for single cells based on a polymer and small molecule have been reported, respectively.[15,16] Recently, PCEs of 9.6% and 10.6% for the tandem solar cells have also been reported by the groups of Janssen and Yang, respectively.[17,18] For the BHJ structured devices, the photovoltaic characteristics are critically dependent on the interfacial properties between the photoactive layer and electrodes.[15,19−23] Therefore, the interfacial modification layers play a key role for efficient solar cells and should be optimized for improving the device's performance.[15,23−26]

Various interface modification materials have been investigated for realizing highly efficient OPVs. For example, the anode electrode (generally indium tin oxide (ITO)) was usually modified with poly(3,4-ethylenedioxythiophene):poly(styrenesulfonate) (PEDOT:PSS) or transition metal oxides (MoO_3, V_2O_5, or NiO),[4,27−29] while the back cathode was typically modified with a thermally evaporated Ca, LiF, Cs_2CO_3, or bathocuproine (BCP) thin layer in high vacuum.[30−32] The modification improved the interfacial properties and consequently minimized the charge carrier extraction losses, thus enhancing device efficiency. The flexible and large scale manufacturing of OPVs via low-cost roll-to-roll technologies requires solution based deposition of all layers in devices. However, Ca or LiF based cathode interface modification is incompatible with the large-area and vacuum-free coating process. Moreover, the high reactivity of Ca with moisture and oxygen makes it unsuitable for wet-deposition techniques.[33,34] Recently, many efforts have been made to replace the use of Ca in OPVs. For example, alcohol or water-soluble conjugated polymer electrolytes have attracted considerable attention due to their potential in cathode interface modification. However, the tedious synthesis and batch-to-batch variation might be the main drawback of their application in OPVs.[26,35] Fullerene derivatives used as cathode buffer layer have also been reported, and excellent performance could be obtained as well. However, they are difficult to synthesize due to the complex chemical structure.[34,36−38]

Received: September 6, 2013
Accepted: December 24, 2013
Published: December 24, 2013

In this work, we demonstrated that insertion of a thin cesium stearate (CsSt) (Figure 1) layer beneath Al electrode as the

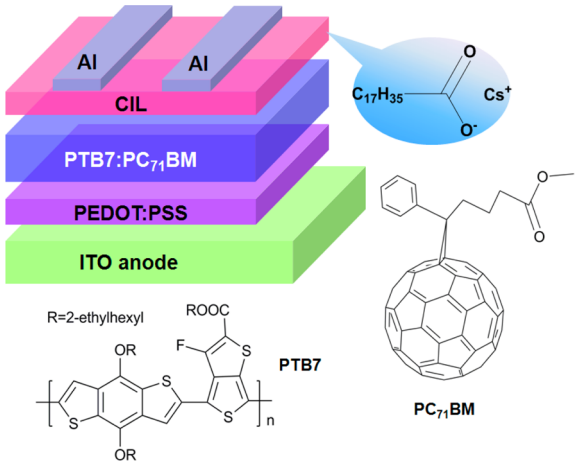

Figure 1. Schematic illustration of the device architecture and the chemical structure of CsSt.

cathode interface modification layer (CIL) can be an effective way to increase the PCE of OPVs from 5.43% to 7.16% (Table 1). The CsSt interlayer was fabricated by spin-coating from *n*-butanol solution. The effectiveness of CsSt as interface modification layer in OPVs was demonstrated. The results indicated that CsSt can improve the device performance effectively.

Table 1. Detailed Characterization of Device Performances with Different Cathode Interfacial Layers

				PCE (%)		
CIL	V_{OC} (V)	J_{SC} (mA cm^{-2})	FF (%)	best	average	R_s (Ω cm^2)
w/o	0.647	15.34	54.7	5.43	5.34	14.22
Ca	0.738	16.30	58.7	7.06	6.72	12.70
CsSt	0.728	16.05	61.3	7.16	6.95	6.26

EXPERIMENTAL SECTION

Materials and Characterization. Indium tin oxide (ITO) coated glass substrates were purchased from Shenzhen Nan Bo Group, China. Poly(3,4-ethylenedioxythiophene):polystyrene sulfonic acid (PEDOT:PSS) (Clevious P VP AI 4083) was purchased from H. C. Stark company. Electron donor material poly[[4,8-bis[(2-ethylhexyl)-oxy]benzo-[1,2-b:4,5-b′]dithiophene-2,6-diyl][3-fluoro-2-[(2-ethyl-hexyl)-carbonyl]-thieno-[3,4-b]thiophenediyl]] (PTB7) and electron acceptor material [6,6]-phenyl-C_{71}-butyric acid methyl ester ($PC_{71}BM$) were purchased from 1-material Chemscitech and ADS, respectively. Chlorobenzene and 1,8-diiodoctane were provided by Sigma-Aldrich. Cs_2CO_3, stearic acid, and *n*-butanol were purchased from Sinopharm Chemical Reagent Co., Ltd. All these commercially available chemicals were used as-received. Cesium stearate was synthesized according to the previous report.[39] Briefly, Cs_2CO_3 and stearic acid (1:2 molar ratio) were added to *n*-butanol and kept refluxing until no more CO_2 formed. Subsequently, *n*-butanol was separated on the rotary evaporator. The residue was mixed with diethyl ether and aspirated.

The current density−voltage characteristics of the photovoltaic devices were recorded using a computer-controlled Keithley 2400 source meter under 1 sun, AM 1.5G simulated solar light. The measurement of external quantum efficiency (EQE) was performed using a IQE200TM data acquisition system. Scanning electron microscopy (SEM) images were conducted on a S-4800 scanning electron microscope operated at an acceleration voltage of 4 kV. An atomic force microscope (AFM) was used to measure film roughness and surface morphologies in tapping mode using a Veeco dimension V atomic microscope at room temperature. Scanning Kelvin probe microscopy (SKPM) measurements were carried out on AFM equipment, using the standard SKPM mode. Droplet images were recorded on a contact-angle system, model OCA20. Thermogravimetric analysis (TGA) was performed on a Perkin-Elmer thermogravimetric/differential thermal analyzer (Pyris Diamond TG/DTA) with a heating rate of 10 °C min^{-1} under nitrogen. Fourier transform infrared (FTIR) spectra were recorded in range of 4000−400 cm^{-1} with Thermo Nicolet 6700 spectroscopy. X-ray powder diffraction (XRD) analyses were performed on a D8 Advance (Bruker AXS) with a Cu Kα (λ = 1.54 Å) radiation source. Electrochemical impedance spectroscopy (EIS) measurements were carried out under dark by applying a 10 mV ac signal over the frequency range of 10^{-1} to 10^5 Hz using an AUTOLAB electrochemical workstation.

Devices Fabrication. The organic bulk heterojunction solar cells studied in our work have a structure of glass/ITO/PEDOT:PSS/PTB7:$PC_{71}BM$/CsSt/Al. The ITO coated glass substrates were precleaned by ultrasonic treatment with a sequence of detergent, deionized water, acetone and isopropanol of 30 min in an ultrasonic bath and then dried with a nitrogen stream. The ITO substrates were then subjected to UV−ozone treatment for 20 min. PEDOT:PSS was spin-coated onto ITO substrates at 4000 rpm for 60 s; then, the film was baked at 140 °C for 20 min on a hot plate in air. All substrates were transferred to the argon-filled glovebox for further processing. Electron donor material PTB7 and electron acceptor material $PC_{71}BM$ (10:15 wt/wt) were weighed (total concentration is 25 mg mL^{-1}) and dissolved in mixed solvents of chlorobenzene/1, 8-diiodoctane (97:3% by volume) in the argon-filled glovebox. The solution was stirred at 60 °C for a minimum of 12 h and spin coated on the freshly prepared PEDOT:PSS interlayers at 2000 rpm for 120 s in the glovebox. The thickness of active layer was around 110 nm. Subsequently, cesium stearate in *n*-butanol solution was spin-coated on top of active layer at 4000 rpm for 60 s. Finally, devices were completed by thermally depositing 100 nm of Al cathode in vacuum under a base pressure of about 1 × 10^{-6} Pa. A shadow mask was used during thermal evaporation to define the active area of 0.04 cm^2.

RESULTS AND DISCUSSION

The device configuration and the chemical structure of CsSt were shown in Figure 1. The Fourier transform infrared (FTIR) spectra were shown in Figure S4, Supporting Information, to analyze the CsSt. It can be seen that the pristine stearic acid showed a sharply characteristic absorption at 1702 cm^{-1} for carbonyl group and that of CsSt showed a typical carboxylate peak at 1564 cm^{-1} and did not show any absorption at 1702 cm^{-1} as stearic acid.[40] The BHJ active materials, PTB7 and $PC_{71}BM$, are used to construct OPVs. Current density−voltage (J−V) characteristics of the devices with CsSt interlayer are presented in Figure 2. The devices without interfacial layer are also fabricated as the control for the comparison. The unique solubility and improved adhesive property of CsSt, due to its long hydrocarbon chain, offer many advantages for its application in electronic devices.[39] In the first step, we optimized the thicknesses of the CsSt layer by changing the concentration of the CsSt *n*-butanol solution from 0.1 to 3 mg mL^{-1}. The optimized processing concentration of CsSt for the high-performance device is 0.5 mg mL^{-1}. The PCE is as high as 7.16% with an open-circuit voltage (V_{OC}) of 0.728 V, a short-circuit current density (J_{SC}) of 16.05 mA cm^{-2}, and a fill factor (FF) of 61.3% (Figure S1, Supporting Information). The results indicated that the effect of the device performance was sensitively dependent on the thickness of the CsSt layer (Table S1, Supporting Information). Specifically, the PCE increased with the rise of CsSt concentration in the range of 0.1 to 0.5 mg

dx.doi.org/10.1021/am403829k | ACS Appl. Mater. Interfaces 2014, 6, 833−838

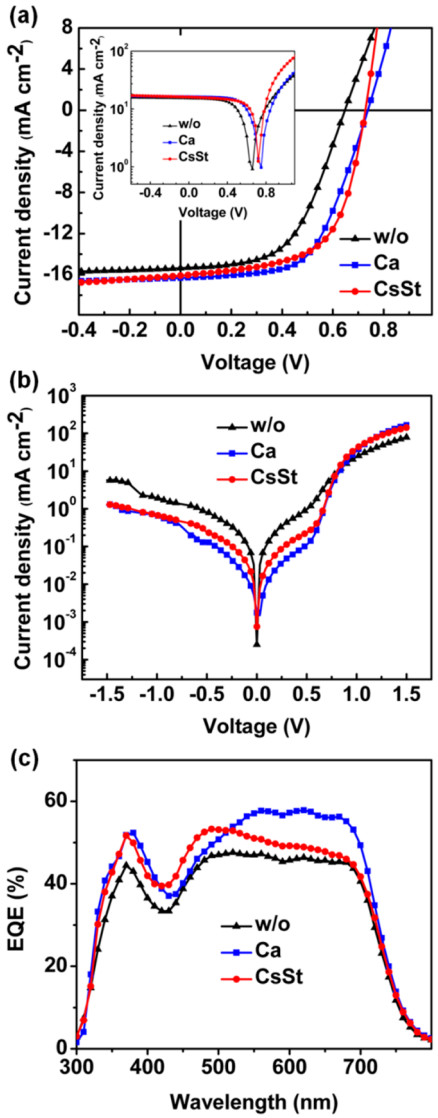

Figure 2. The effect of the CsSt interlayer on solar cell performance. Current density–voltage (J–V) characteristics of the devices without and with Ca or CsSt interfacial layer (a) measured under illumination and (b) in the dark. (c) EQE spectra of solar cells without and with Ca or CsSt interfacial layer.

mL^{-1}. However, when the CsSt concentration was higher than 0.5 mg mL^{-1}, the PCEs of the devices were inversely decreased. When the concentration is up to 3 mg mL^{-1}, the efficiency drops to 2.56%, with the dramatic decrease of J_{SC} (9.60 mA cm^{-2}) and FF (37.9%). A thicker CsSt layer would prohibit the charge injection from photoactive layer to cathode due to the increase in series resistance (R_s), since it is insulating. Compared to the control devices, incorporation of the CsSt with optimized thickness leads to a simultaneous enhancement of V_{OC} (0.728 vs 0.647 V), J_{SC} (16.05 vs 15.34 mA cm^{-2}), and FF (61.3% vs 54.7%), corresponding to an obvious improvement in the device PCE by 31.86% (7.16% vs 5.43%). In order to check the reproducibility of the device, ten devices using the CsSt interfacial layer were examined under the same condition. The maximum and average PCE were 7.16% and 6.95%, respectively, which suggested the devices could present excellent performance and favorable reproducibility by using the solution-processed CsSt as cathode interfacial layer. The PCE of CsSt based device is also better than that of the Ca based one (PCE = 7.06%), suggesting the superior interfacial properties of the CsSt layer. The external quantum efficiency (EQE) spectra of the device with and without the CsSt interlayer were measured (Figure 2c). As can be seen, the device with the CsSt interlayer exhibited a substantial enhancement response from the wavelength range of 320 to 700 nm as compared with that one without CsSt interlayer. As shown in Figure 2a, a large forward current was observed in the device with CsSt interlayer than that without interlayer. This indicated that the interface between active layer and Al cathode was improved by inserting the CsSt layer. Therefore, an enhanced EQE response was observed from the photovoltaic device with CsSt interlayer.

The increase of V_{OC} in the devices might be attributed to the dipole induced by the thin CsSt interlayer. Very recently SKPM has been used to probe interfacial dipole induced by different interfacial layers for BHJ OSCs, and the direction of dipole moment can be simply deduced from the value of surface potential change upon the incorporation of interlayers.[25] SKPM measures two-dimensional distributions of contact potential difference between the tip and the sample.[41] To visualize the interfacial dipole upon the incorporation of the CsSt layer, the surface potentials of blend films with and without CsSt interlayer are probed by SKPM. As shown in Figure 3, the

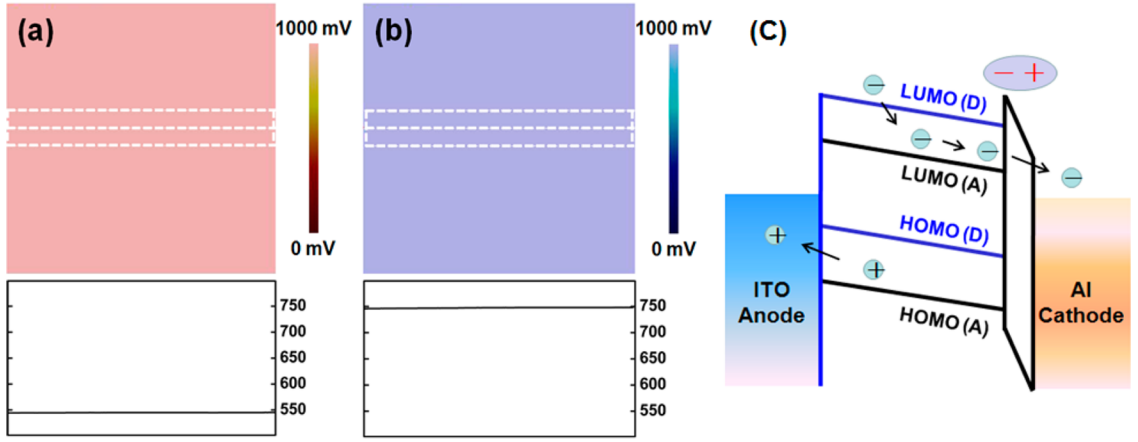

Figure 3. Surface potential images of the PTB7:PC$_{71}$BM film (a) without and (b) with CsSt interfacial layer. (c) The energy band structure of the devices.

dx.doi.org/10.1021/am403829k | ACS Appl. Mater. Interfaces 2014, 6, 833–838

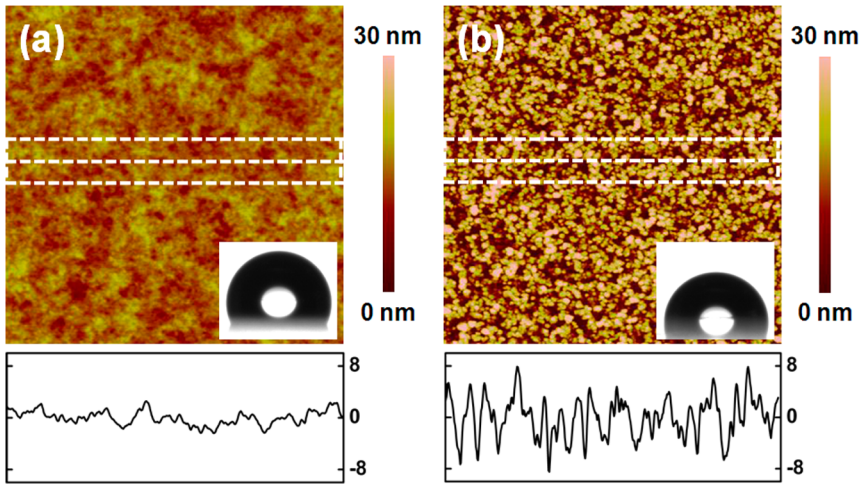

Figure 4. The AFM height images and surface profiles (−8 to 8 nm) of (a) PTB7:$PC_{71}BM$ and (b) CsSt interlayer coated on PTB7:$PC_{71}BM$ film with a scan size of 5 μm × 5 μm. Photographs of water droplets on both surfaces are given as insets.

surface potentials are uniform for both layers, but the potential of the PTB7:$PC_{71}BM$ film incorporated CsSt interlayer is about 200 mV more positive than that of the PTB7:$PC_{71}BM$ film without interlayer, which is similar to the case of PFN interlayer.[25] The surface potential is an extremely sensitive indicator of surface condition and can be affected by electronic states on the surface including surface reconstruction and chemical composition.[41,42] The 200 mV positive shifts of the surface potential upon the incorporation of CsSt compared to the reference PTB7:$PC_{71}BM$ film indicate that a CsSt-induced microscopic electric dipole moment exists with the positive charge end pointing toward the Al cathode and the negative charge end pointing toward the PTB7:$PC_{71}BM$ photoactive layer.[25,43,44] The dipole moment might arise from the rearrangement of positive and negative charges of CsSt, in which part of the molecule has a more positive charge and the other part has a more negative one, which could cause electrical asymmetry. The direction of this dipole moment is aligned with the built-in potential. Therefore, the actual built-in potential across the device is reinforced. Many studies have also reported that the dipole layer could be used to adjust the work function of the interface.[45−48] As a result, the energy level offset between the Al cathode and the electron acceptor $PC_{71}BM$ is decreased (Figure 3c), which will facilitate the electron extraction.[25,49] Thus, the incorporation of CsSt exerts an additional electrical field at the interface between photoactive layer and Al cathode, resulting in an increase of V_{OC}. In addition, the reduction of R_s in the device with CsSt can further ensure a higher V_{OC} due to the decrease of the potential drop at the interface of active layer and cathode. Along with the enhancement of V_{OC} and J_{SC}, the FF is found to be 61.3%, higher than that of the control device (54.7%), suggesting the improvement of charge transport properties as well. All these are responsible for the efficiency enhancement of the devices with CsSt interface modification layer. To further scrutinize the electrical characteristics of the devices, $J-V$ curves of the devices with and without CsSt interface layer in the darkness are presented in Figure 2b. Evidently, the control device shows a low current in the forward direction and high leakage current in the reverse direction. However, the CsSt based device exhibits excellent diode characteristics with a low leakage current and series resistance, which is favorable for the electron extraction. Thus, the reduced leakage current and series resistance compared to control device also contributed to the increase in J_{SC} for the CsSt based device.

The surface morphologies of the blend thin film with and without CsSt interlayer are studied by SEM (Figure S2, Supporting Information). The surface of pristine PTB7:$PC_{71}BM$ film was quite smooth (Figure S2a, Supporting Information). When the PTB7:$PC_{71}BM$ film was covered by CsSt molecules, clearly there was an additional layer on top of the active layer. This result indicates the formation of CsSt layer on the surface of PTB7:$PC_{71}BM$ layer due to the aggregation of CsSt molecules. The formation mechanism of such aggregation domains is not clear. It could relate to the self-assembly of CsSt on the PTB7:$PC_{71}BM$ layer, because CsSt is more hydrophilic than PTB7 and $PC_{71}BM$, which is confirmed by the water contact angle measurements. Figure 4 showed the water contact angle of the PTB7:$PC_{71}BM$ layer before and after the deposition of the CsSt interlayer. The contact angle of the PTB7:$PC_{71}BM$ layer surface prior to the deposition of CsSt was 120°. After deposition of CsSt, it was 107°, which was 13° smaller than that of the PTB7:$PC_{71}BM$ layer without a CsSt layer. This result further indicated that the hydrophilic CsSt interlayer was on the surface of the PTB7:$PC_{71}BM$ layer and the interface was improved. AFM was then employed to further investigate the surface of blend film. As we can see from Figure 4a, the surface morphology of pristine PTB7:$PC_{71}BM$ showed separated nanodomains, and the film was smooth, with a root-mean-square (rms) roughness of 2.3 nm at a scan scale of 5 μm × 5 μm. However, the PTB7:$PC_{71}BM$/CsSt layer showed a rough surface with many obvious protrusions. The nanodomain features resulting from the microphase separation became less discernible. The surface rms roughness of the PTB7:$PC_{71}BM$/CsSt layer increases to 9.1 nm with height of 8−15 nm (Figure 4b). The rough surface offers a better interface and increases the contact area between interlayer and Al cathode, which contributes to the electron extraction and collection.

To illustrate the effects of the CsSt interlayer on the charge collection efficiency, we also determined the maximum exciton generation rate (G_{max}) and exciton dissociation probabilities (P) of our devices. Figure S7, Supporting Information, reveals the effect of CsSt on the photocurrent density (J_{ph}) versus the effective voltage (V_{eff}). J_{ph} is determined as $J_{ph} = J_L - J_D$, where J_L and J_D are the current density under illumination and in the dark, respectively. V_{eff} is determined as $V_{eff} = V_0 - V_a$, where V_0

dx.doi.org/10.1021/am403829k | ACS Appl. Mater. Interfaces 2014, 6, 833−838

is the voltage at which $J_{ph} = 0$ and V_a is the applied voltage.[50−52] Figure S7, Supporting Information, clearly shows that J_{ph} increases at low V_{eff} range and at a large voltage (V_{eff} = 1.5 V) J_{ph} reaches saturation for both devices. It suggests that all the photogenerated excitons dissociated into free charge carriers and were collected at the electrodes. In this case, saturation current density (J_{sat}) is only limited by the amount of absorbed incident photons. Thus, the G_{max} could be given by $J_{ph} = qG_{max}L$, where q is the electronic charge and L is the thickness of active layer (110 nm).[51,52] The values of G_{max} for the device without and with CsSt interface modification layer are 9.99×10^{27} m^{-3} s^{-1} (J_{sat} = 176.1 A m^{-2}) and 10.24×10^{27} m^{-3} s^{-1} (J_{sat} = 180.4 A m^{-2}), respectively. The P values could be obtained from the ratio of J_{ph}/J_{sat}. P values under J_{sc} condition are 87% and 89% for device without and with CsSt interlayer, respectively. Interestingly, in the low effective voltage range, the P values for the two devices show large differences. For example, at 0.2 V of V_{eff}, P is 69% for the device without interlayer while it is 74% for the device with CsSt interlayer. Since P value is the exciton dissociation efficiency, a lower P value indicates a reduced exciton dissociation efficiency. It suggests that exciton recombination begins to dominate the process and thus leads to a lower fill factor in the device without CsSt interlayer.[25] The $J_{ph}-V_{eff}$ characteristics from devices with CsSt interfacial layer identify the effect of CsSt on reducing exciton recombination and benefitting the dissociation of excitons into free charge carriers at the low effective voltage.

To explore the influence of incorporation of CsSt interfacial layer on the charge recombination, the devices without and with CsSt interfacial layer were also analyzed by EIS measurement (Figure S9, Supporting Information). The recombination resistance plots of the two devices were calculated out by fitting the impedance spectra. It was obtained that the CsSt based device has higher recombination resistance than the device without CsSt interfacial layer, so we concluded that the charge recombination was retarded due to the incorporation of the CsSt interfacial layer.

To investigate the effect of the CsSt on the device stability, we performed the lifetime measurement of the CsSt based device. Figure S8, Supporting Information, showed the normalized efficiency of CsSt and Ca based devices versus storage time. The devices were stored in the argon-filled glovebox without encapsulation. As the data showed, the CsSt based device degraded slower than the Ca based device did within 40 h. Compared to the Ca, the CsSt interlayer gave better device stability.

CONCLUSION

In conclusion, we have developed solution-processed cesium stearate as the interface modification material between the photoactive layer and metal cathode to improve the device performance of organic photovoltaics. The resulting cesium stearate possessed integrated advantages of good solubility, simplicity of process, and interface modification functions. The SKPM measurement revealed that the cesium steatate interfacial layer induced a dipole layer, which caused the decrease of energy level offset between photoactive layer and Al cathode. As a result, PCE of devices was remarkably improved compared to those devices without interfacial layer, which was also higher than the conventional device using Ca as interlayer. Our results showed promising potentials of cesium stearate as a cathode interface modification material in organic photovoltaics and provided new insights for the development of new interface modification materials.

ASSOCIATED CONTENT

Supporting Information

Current density−voltage ($J-V$) characteristics of the devices with CsSt cathode interfacial layer from different concentrations, detailed parameters of device performance, SEM images, the three-dimension AFM images, FTIR, XRD pattern, thermogravimetric analysis, photocurrent density (J_{ph}) versus effective voltage (V_{eff}) characteristics, normalized device efficiency as a function of storage time, and impedance spectra of the devices without or with CsSt interfacial layer. This material is available free of charge via the Internet at http://pubs.acs.org.

AUTHOR INFORMATION

Corresponding Authors

*E-mail: jiutonggang@nimte.ac.cn (T.J.).
*E-mail: fangjf@nimte.ac.cn (J.F.).
*E-mail: fslu@stu.edu.cn (F.L.).

Notes

The authors declare no competing financial interest.

ACKNOWLEDGMENTS

The authors gratefully acknowledge the support of the National Natural Science Foundation of China (No. 51202264 and 51273208) and the Specialized Research Fund for the Spring Buds Talent Program (No. Y20804RA02). The work was also supported by Hundred Talent Program of Chinese Academy of Science, the Ningbo Natural Science Foundation of China (2012A610114), and the Open Fund of the State Key Laboratory of Luminescent Materials and Devices (South China University of Technology).

REFERENCES

(1) Li, G.; Shrotriya, V.; Huang, J.; Yao, Y.; Moriarty, T.; Emery, K.; Yang, Y. *Nat. Mater.* **2005**, *4*, 864−868.
(2) Günes, S.; Neugebauer, H.; Sariciftci, N. S. *Chem. Rev.* **2007**, *107*, 1324−1338.
(3) Thompson, B. C.; Fréchet, J. M. J. *Angew. Chem., Int. Ed.* **2008**, *47*, 58−77.
(4) Chen, H.-Y.; Hou, J.; Zhang, S.; Liang, Y.; Yang, G.; Yang, Y.; Yu, L.; Wu, Y.; Li, G. *Nat. Photonics* **2009**, *3*, 649−653.
(5) Kaltenbrunner, M.; White, M. S.; Głowacki, E. D.; Sekitani, T.; Someya, T.; Sariciftci, N. S.; Bauer, S. *Nat. Commun.* **2012**, *3*, 770.
(6) Zhou, J.; Wan, X.; Liu, Y.; Zuo, Y.; Li, Z.; He, G.; Long, G.; Ni, W.; Li, C.; Su, X.; Chen, Y. *J. Am. Chem. Soc.* **2012**, *134*, 16345−16351.
(7) Fan, X.; Cui, C.; Fang, G.; Wang, J.; Li, S.; Cheng, F.; Long, H.; Li, Y. *Adv. Funct. Mater.* **2012**, *22*, 585−590.
(8) Ma, W.; Yang, C.; Gong, X.; Lee, K.; Heeger, A. J. *Adv. Funct. Mater.* **2005**, *15*, 1617−1622.
(9) Blom, P. W. M.; Mihailetchi, V. D.; Koster, L. J. A.; Markov, D. E. *Adv. Mater.* **2007**, *19*, 1551−1566.
(10) Liang, Y.; Xu, Z.; Xia, J.; Tsai, S.-T.; Wu, Y.; Li, G.; Ray, C.; Yu, L. *Adv. Mater.* **2010**, *22*, E135−E138.
(11) Ma, W.; Gopinathan, A.; Heeger, A. J. *Adv. Mater.* **2007**, *19*, 3656−3659.
(12) So, F.; Kondakov, D. *Adv. Mater.* **2010**, *22*, 3762−3777.
(13) Coakley, K. M.; McGehee, M. D. *Chem. Mater.* **2004**, *16*, 4533−4542.
(14) Yang, X.; Loos, J.; Veenstra, S. C.; Verhees, W. J. H.; Wienk, M. M.; Kroon, J. M.; Michels, M. A. J.; Janssen, R. A. J. *Nano Lett.* **2005**, *5*, 579−583.

(15) He, Z.; Zhong, C.; Su, S.; Xu, M.; Wu, H.; Cao, Y. *Nat. Photonics* **2012**, *6*, 591−595.
(16) Wang, D. H.; Kyaw, A. K. K.; Gupta, V.; Bazan, G. C.; Heeger, A. J. *Adv. Energy Mater.* **2013**, *3*, 1161−1165.
(17) Li, W.; Furlan, A.; Hendriks, K. H.; Wienk, M. M.; Janssen, R. A. J. *J. Am. Chem. Soc.* **2013**, *135*, 5529−5532.
(18) You, J.; Dou, L.; Yoshimura, K.; Kato, T.; Ohya, K.; Moriarty, T.; Emery, K.; Chen, C.-C.; Gao, J.; Li, G.; Yang, Y. *Nat. Commun.* **2013**, *4*, 1446.
(19) Manders, J. R.; Tsang, S.-W.; Hartel, M. J.; Lai, T.-H.; Chen, S.; Amb, C. M.; Reynolds, J. R.; So, F. *Adv. Funct. Mater.* **2013**, *23*, 2993−3001.
(20) Xie, F.; Choy, W. C. H.; Wang, C.; Li, X.; Zhang, S.; Hou, J. *Adv. Mater.* **2013**, *25*, 2051−2055.
(21) Tan, Z.; Qian, D.; Zhang, W.; Li, L.; Ding, Y.; Xu, Q.; Wang, F.; Li, Y. *J. Mater. Chem. A* **2013**, *1*, 657−664.
(22) Yip, H.-L.; Jen, A. K. Y. *Energy Environ. Sci.* **2012**, *5*, 5994−6011.
(23) Yang, T.; Wang, M.; Duan, C.; Hu, X.; Huang, L.; Peng, J.; Huang, F.; Gong, X. *Energy Environ. Sci.* **2012**, *5*, 8208−8214.
(24) Graetzel, M.; Janssen, R. A. J.; Mitzi, D. B.; Sargent, E. H. *Nature* **2012**, *488*, 304−312.
(25) He, Z.; Zhong, C.; Huang, X.; Wong, W.-Y.; Wu, H.; Chen, L.; Su, S.; Cao, Y. *Adv. Mater.* **2011**, *23*, 4636−4643.
(26) Seo, J. H.; Gutacker, A.; Sun, Y.; Wu, H.; Huang, F.; Cao, Y.; Scherf, U.; Heeger, A. J.; Bazan, G. C. *J. Am. Chem. Soc.* **2011**, *133*, 8416−8419.
(27) Murase, S.; Yang, Y. *Adv. Mater.* **2012**, *24*, 2459−2462.
(28) Zilberberg, K.; Trost, S.; Schmidt, H.; Riedl, T. *Adv. Energy Mater.* **2011**, *1*, 377−381.
(29) Steirer, K. X.; Ndione, P. F.; Widjonarko, N. E.; Lloyd, M. T.; Meyer, J.; Ratcliff, E. L.; Kahn, A.; Armstrong, N. R.; Curtis, C. J.; Ginley, D. S.; Berry, J. J.; Olson, D. C. *Adv. Energy Mater.* **2011**, *1*, 813−820.
(30) Brabec, C. J.; Shaheen, S. E.; Winder, C.; Sariciftci, N. S.; Denk, P. *Appl. Phys. Lett.* **2002**, *80*, 1288−1290.
(31) Chang, C.-C.; Lin, C.-F.; Chiou, J.-M.; Ho, T.-H.; Tai, Y.; Lee, J.-H.; Chen, Y.-F.; Wang, J.-K.; Chen, L.-C.; Chen, K.-H. *Appl. Phys. Lett.* **2010**, *96*, 263506.
(32) Huang, J.; Xu, Z.; Yang, Y. *Adv. Funct. Mater.* **2007**, *17*, 1966−1973.
(33) Zhang, F.; Ceder, M.; Inganäs, O. *Adv. Mater.* **2007**, *19*, 1835−1838.
(34) Zhang, Z.-G.; Li, H.; Qi, Z.; Jin, Z.; Liu, G.; Hou, J.; Li, Y.; Wang, J. *Appl. Phys. Lett.* **2013**, *102*, 143902.
(35) Duan, C.; Zhang, K.; Guan, X.; Zhong, C.; Xie, H.; Huang, F.; Chen, J.; Peng, J.; Cao, Y. *Chem. Sci.* **2013**, *4*, 1298−1307.
(36) Li, S.; Lei, M.; Lv, M.; Watkins, S. E.; Tan, Z. a.; Zhu, J.; Hou, J.; Chen, X.; Li, Y. *Adv. Energy Mater.* **2013**, *3*, 1569−1574.
(37) Mei, Q.; Li, C.; Gong, X.; Lu, H.; Jin, E.; Du, C.; Lu, Z.; Jiang, L.; Meng, X.; Wang, C.; Bo, Z. *ACS Appl. Mater. Interfaces* **2013**, *5*, 8076−8080.
(38) Zhang, Z.-G.; Li, H.; Qi, B.; Chi, D.; Jin, Z.; Qi, Z.; Hou, J.; Li, Y.; Wang, J. *J. Mater. Chem. A* **2013**, *1*, 9624−9629.
(39) Wetzelaer, G. A. H.; Najafi, A.; Kist, R. J. P.; Kuik, M.; Blom, P. W. M. *Appl. Phys. Lett.* **2013**, *102*, 053301.
(40) Pudney, P. D. A.; Mutch, K. J.; Zhu, S. *Phys. Chem. Chem. Phys.* **2009**, *11*, 5010−5018.
(41) Pingree, L. S. C.; Reid, O. G.; Ginger, D. S. *Adv. Mater.* **2009**, *21*, 19−28.
(42) Zhou, H.; Zhang, Y.; Seifter, J.; Collins, S. D.; Luo, C.; Bazan, G. C.; Nguyen, T.-Q.; Heeger, A. J. *Adv. Mater.* **2013**, *25*, 1646−1652.
(43) Zhang, W.; Wang, H.; Chen, B.; Bi, X.; Venkatesan, S.; Qiao, Q.; Yang, S. *J. Mater. Chem.* **2012**, *22*, 24067−24074.
(44) Wang, H.; Zhang, W.; Xu, C.; Bi, X.; Chen, B.; Yang, S. *ACS Appl. Mater. Interfaces* **2012**, *5*, 26−34.
(45) Osikowicz, W.; de Jong, M. P.; Salaneck, W. R. *Adv. Mater.* **2007**, *19*, 4213−4217.
(46) Crispin, X.; Geskin, V.; Crispin, A.; Cornil, J.; Lazzaroni, R.; Salaneck, W. R.; Brédas, J.-L. *J. Am. Chem. Soc.* **2002**, *124*, 8131−8141.
(47) de Boer, B.; Hadipour, A.; Mandoc, M. M.; van Woudenbergh, T.; Blom, P. W. M. *Adv. Mater.* **2005**, *17*, 621−625.
(48) Yip, H.-L.; Hau, S. K.; Baek, N. S.; Ma, H.; Jen, A. K. Y. *Adv. Mater.* **2008**, *20*, 2376−2382.
(49) Braun, S.; Salaneck, W. R.; Fahlman, M. *Adv. Mater.* **2009**, *21*, 1450−1472.
(50) Shrotriya, V.; Yao, Y.; Li, G.; Yang, Y. *Appl. Phys. Lett.* **2006**, *89*, 063505.
(51) Chen, F.-C.; Wu, J.-L.; Lee, C.-L.; Hong, Y.; Kuo, C.-H.; Huang, M. H. *Appl. Phys. Lett.* **2009**, *95*, 013305.
(52) Xu, M.-F.; Zhu, X.-Z.; Shi, X.-B.; Liang, J.; Jin, Y.; Wang, Z.-K.; Liao, L.-S. *ACS Appl. Mater. Interfaces* **2013**, *5*, 2935−2942.